CrossMark

ORIGINAL PAPER

Impact indicators for caprock integrity and induced seismicity in CO_2 geosequestration: insights from uncertainty analyses

Xiaochen Wei[1] · Qi Li[1] · Xiaying Li[1] · Yankun Sun[1]

Abstract The geological sequestration (geosequestration) of carbon dioxide (CO_2) is a mitigation method for reducing greenhouse gas emission into the atmosphere. The security and safety of CO_2 geosequestration are strongly dependent on the mechanical stability of the caprock overlying the reservoir. Underground injection of CO_2 increases the pore pressure and thus decreases the effective stress. It may lead to caprock failure, as well as the subsequent leakage of sequestered CO_2. In particular, geothermal exploitation and the underground disposal of hazardous liquid wastes have demonstrated a risk of induced seismicity. We performed an uncertainty analysis using a novel response surface methodology and a two-step statistical experimental design, evaluated the statistical significance of operator choices and subsurface uncertainties to caprock integrity, and quantified the moment magnitude of the induced seismicity. Furthermore, the optimal combination (i.e., the worst-case scenario) with the desired properties was forecast. A series of numerical experiments was well designed, and 130 combinations were statistically determined. Based on the results from the analysis of variance for the response surface quadratic model, the impact indicators were presented in histograms according to their significances to the Coulomb failure stress and moment magnitude of the induced seismicity. Lastly, the values of the selected independent impact indicators were predicted to obtain optimal compositions for object function of both Coulomb failure stress and moment magnitude, and the desired properties were being picked out. The optimal combinations had desirability values of 1.000, demonstrating the fitness of the selected statistical models in analyzing the experimental data.

✉ Qi Li
  qli@whrsm.ac.cn

[1] State Key Laboratory of Geomechanics and Geotechnical Engineering, Institute of Rock and Soil Mechanics, Chinese Academy of Sciences, Wuhan 430071, China

1 Introduction

Carbon dioxide (CO_2) capture and storage (CCS) is considered as an option for reducing the atmospheric emissions of CO_2 and mitigating the greenhouse effects on the environment, as well as enhancing energy and resources recovery (e.g., IPCC 2005; Liu and Wu 2015; Mathias et al. 2009). CO_2 geosequestration is widely regarded as an effective technology for the reduction in greenhouse gas emissions to alleviate climate change (Deng et al. 2012; Li et al. 2014c; Wei et al. 2015). However, the considerable quantities of supercritical CO_2 that are injected into deep geological formations can create large overpressures and subsequent changes in the state of stress that may jeopardize the caprock mechanical stability and could generate a leakage path for CO_2 (Bachu 2000; Song and Zhang 2013). This overpressure may induce microseismic events if the caprock yields, which could also open a leakage path for CO_2 (Vilarrasa 2014). The leaked CO_2 could affect both human health and groundwater and even threaten the ecosystem balance (Li et al. 2014b). Thus, it is necessary to have sufficient knowledge of the caprock and its long-term integrity to ensure the long-term storage of CO_2 in deep saline formations or depleted hydrocarbon reservoirs.

In recent years, the issues involved in underground CO_2 sequestration have been discussed in the scientific literature mainly from fluid property (Hosein and Alshakh 2013), fluid interaction (Gysi and Stefánsson 2012; Lei and Ma 2013), and geochemical viewpoints (Dethlefsen et al. 2011). Regarding CO_2 injection, many attempts have been made to examine the related geomechanical processes, particularly caprock integrity, during CO_2 injection (Karimnezhad et al. 2014; Li et al. 2014a; Vidal-Gilbert et al. 2009; Vilarrasa 2014). The following concerns have recently been raised: (1) CO_2 injection at a scale that is necessary to curb increases in the atmospheric CO_2 will inevitably lead to the reactivation of moderately sized faults that compromise caprock integrity (Seebeck et al. 2015; Zhou and Burbey 2014) and may even trigger notable seismic events; and (2) it is unclear how such events could impact the long-term integrity of a CO_2 repository (Cappa and Rutqvist 2011). Zoback and Gorelick (2012) reported a high probability that earthquakes would be triggered by the injection of large volumes of CO_2 into the brittle rocks that are commonly observed in continental interiors, and because even small to moderately sized earthquakes threaten the seal integrity of CO_2 repositories, large-scale CCS would be a risky and likely unsuccessful strategy for significantly reducing greenhouse gas emissions into the atmosphere (Lary et al. 2015; Wei et al. 2015). Studies of the actual CO_2 injection sites, such as the In Salah in Algeria, have demonstrated that significant geomechanical changes may indeed occur depending on the injection pressure and the site-specific geomechanical conditions (Rutqvist 2012; Zhou et al. 2010). It is clear that modeling the magnitude of injection-related stresses and the associated property changes in the caprock, reservoir, and fault are crucial to understanding and surmounting this particular challenge facing CCS (Dempsey et al. 2014; Rohmer et al. 2014; Tenthorey et al. 2014).

In this study, we performed coupled flow and stress numerical modeling of CO_2 injection to investigate the potential for caprock instability and induced seismicity

(Rohmer 2014). If the seismicity occurs, the operator needs to do the enhanced monitoring, to do the detailed geomechanical assessment, and to check related emergence management measures. This research is important not only concerning artificial reservoir problems such as CO_2 geosequestration or underground energy storage but also for researchers of subsurface fluid flow triggered natured earthquake processes. This study provides novelty in three aspects: (1) the distributions of Coulomb failure stress (CFS) that describe the fault stability and (2) in case of reactivation the moment magnitude of the associated seismic event. (3) Response surface methodology with a Box–Behnken experimental design was used to investigate the statistical significance of indicators of CFS as well as the moment magnitude of the induced seismicity and predicted the optimal design of the subsurface uncertainties. Our recent published paper in Engineering Geology (Wei et al. 2015) is to investigate an uncertainty analysis of nine impact indicators. It proved the Box–Behnken design and response surface methodology could efficiently be applied in uncertainty analyses of caprock integrity and induced seismicity in CO_2 geosequestration. On this basis, we focus on a more complex situation that we usually encountered in site selection stage. Compared with our previous work, this study provides novelty in three aspects: (1) A 200-m fault with a 60° dip angle penetrates the caprock into the reservoir, and contact between fault and surrounding rock and fault slip have to be taken into consideration. (2) Based on a large number of 22-input tested parameters that exert major effects, which are beyond the upper limitation of the Box–Behnken design, to settle this problem, before the application of Box–Behnken design and response surface mapping, we used a tornado analysis to determine which tested parameters have the greatest influence on the simulated results, and only the parameters that show observable sensitivity go to the next step. (3) In case of reactivation, the moment magnitude of the associated seismic event was evaluated. Response surface methodology with a Box–Behnken experimental design was used to investigate the statistical significance of indicators of the moment magnitude of the induced seismicity, and the optimal design of the subsurface uncertainties was predicted. The results are more constructive in the site selection process. In Sect. 2, the geometry and the failure properties are described in detail. Section 3 details the study methodology, including a description of the response surface mapping that was used to investigate the statistical significance of the different tested parameters (Sect. 3.1), and the statistical experimental design for the tests performed, including tornado analysis and Box–Behnken experimental design (Sect. 3.2). In Sect. 4, we describe the statistical significance and optimal design of tested parameters for both Coulomb failure stress and the moment magnitude of the induced seismicity (Sects. 4.1 and 4.2). The primary findings and conclusions of this study are then summarized in Sect. 5.

2 Geomechanical model

2.1 Geometry and mesh of the model

The application of geomechanical models contributes significantly to the calculation of the stress distribution after CO_2 injection (Aruffo et al. 2014; Dethlefsen et al. 2011; Xing et al. 2015; Yang et al. 2012). To solve the coupling between fluid flow and geomechanical problems, different approaches can be used (Fei et al. 2015; Jeannin et al. 2007; Rutqvist et al. 2002). The fully coupled approach simultaneously solves the whole set of equations that govern the hydromechanical problem. And the partially coupled approach is based on an

external coupling between conventional reservoir and geomechanical simulators. One-way coupled approach is the simplest partially coupled approach in which the pore pressure history issued from a conventional reservoir simulation is introduced as input into the geomechanical equilibrium equation. In practice, the pore pressure computed by reservoir simulation is introduced in poroelasticity equations to deduce stress and deformation. This coupling is easy to be implemented and still includes interesting physics (Fei et al. 2015; Vidal-Gilbert et al. 2009).

In this study, we focus on the effect of fluid injection with low pore pressure variation, and the effect of deformation on porosity is expected to be insignificant and therefore a fully coupled model is not necessary. Hence, the one-way coupling technique has been chosen without multiphase flow processes, and a two-dimensional (2D) numerical model was used to consider the geomechanical aspects of the injection of CO_2 into the reservoir to simulate the storage of CO_2 through injections from a single well into the deep saline formations in the Ordos Basin, China. Rock masses are discontinuous and have hetero-geneous and anisotropic properties, and their mechanical properties are greatly depending on the types of rock, buried depths, geological, and diagenetic processes (Jaeger et al. 2009; Zhou and Burbey 2014). For evaluating the coupled fluid and mechanical behavior of these coupled systems, we use the theory of poroelasticity as a very practical and powerful mathematical approach (Biot 1956; Coussy 2004).

As the most complete and stable structural unit in China, the Ordos Basin is an ideal site for a CCS project (Liu et al. 2009). The Shenhua demonstration CCS project is located in Inner Mongolia, and the target zone is located in the backfill area of the Shenhua open pit coal mine in the western riverbed of the Ulan Moron River. This area is approximately 45 km southeast of the Ordos city, Inner Mongolia, China, and 1.3 km east of the Shenhua Ordos Coal to Oil Branch (Li et al. 2014a). Figure 1 shows a schematic view of the model geometry, where only the main geological units are represented: Ordovician, Carbonifer-ous, Permian, and Triassic (Li et al. 2013). The target layer is 1620 m thick. Based on the lithology histogram, the geometric model was obtained by ignoring the thin layers of the reservoir and caprock.

The geometry of the 2D model is rectangular with a length of 3000 m; therefore, the outer boundary does not significantly affect the mechanical behavior of the model. According to the geological depth, the numerical model extends vertically from −780 to −2400 m, and the formations below 780 m can be divided into three primary reservoir–seal combinations (Fig. 1). Fluid is injected into the storage reservoir from a vertical injection well located on the left of the model at a constant injection pressure of 4.5 MPa for 15 days. A 200-m fault with a 60° dip angle penetrates the caprock into the reservoir. The coefficient of friction on the fault was set to 0.6, and the distance from the injection well to the left boundary of the fault is 1000 m. To enhance the computational accuracy and efficiency, a structured mesh with 5990 elements was adopted in the numerical model. And four-node reduced integration and pore pressure elements were used to mesh the model. Figure 2 presents the pore pressure nephograms in the targeted reservoir and the fault at different time. The pore pressure rises from the leftmost boundary from the injection point and spreads to right with time.

2.2 Failure properties

To determine whether the preexisting fault affecting the caprock is stable during CO_2 injection, a failure criterion must be defined. A failure criterion defines a domain in the
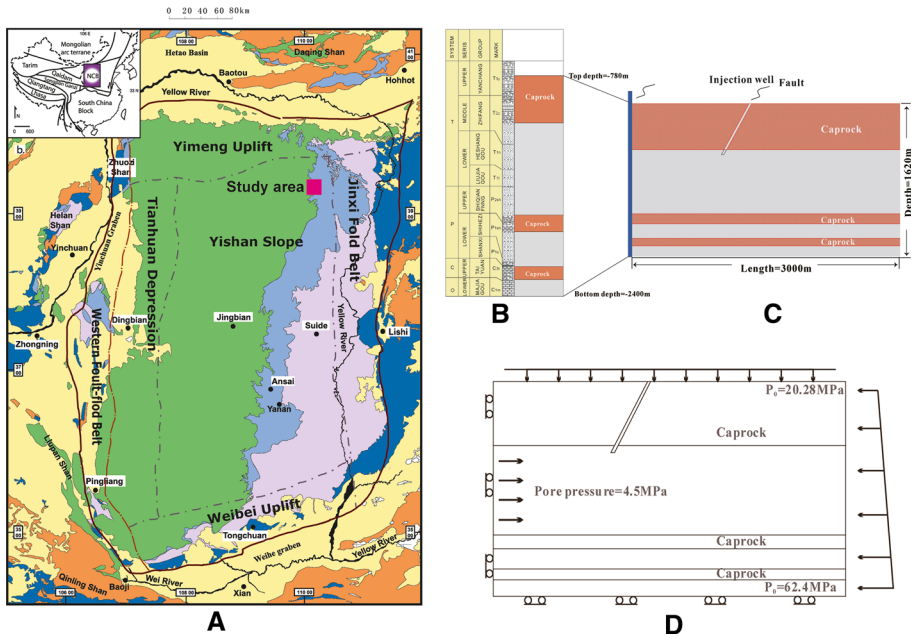
Fig. 1 Geological model and numerical model of the target layers in the Ordos Basin. **A** Location of Ordos Basin and the study area (*purple square*). **B**, **C** Reservoir–seal combinations and the corresponding numerical model, respectively. The injection well located on the *left boundary* of the numerical model. And the boundary conditions used in the numerical model are illustrated in **D**

stress space outside of which the rock cannot withstand the load (Vidal-Gilbert et al. 2009). A failure criterion is commonly addressed by Mohr–Coulomb's approach:

$$\tau = c + \sigma' \tan \varphi \tag{1}$$

where τ and σ' are the shear stress and normal effective stress, respectively, on the fault through which material failure occurs, and c and φ are the cohesion and the angle of the internal friction of the fault, respectively. In this study, the Mohr–Coulomb failure criterion was included to simulate the effects of rock failure. According to the Mohr–Coulomb failure criterion, a necessary condition for fault instability is the Coulomb failure stress (CFS) reaching or exceeding its breaking strength (S):

$$\text{CFS} = \tau + \tan \varphi (\sigma - P_f) \geq S \tag{2}$$

where τ is the shear stress that causes sliding, σ is the normal effective stress, and P_f is the pore pressure. In the presence of a fault, we focused on the CFS in the fault generated with the fluid injection.

3 Methodology

3.1 Response surface methodology

Response surface methodology (RSM), which was developed by Box and Hunter in the 1950s (Box and Hunter 1957), is a collection of statistical and mathematical methods that
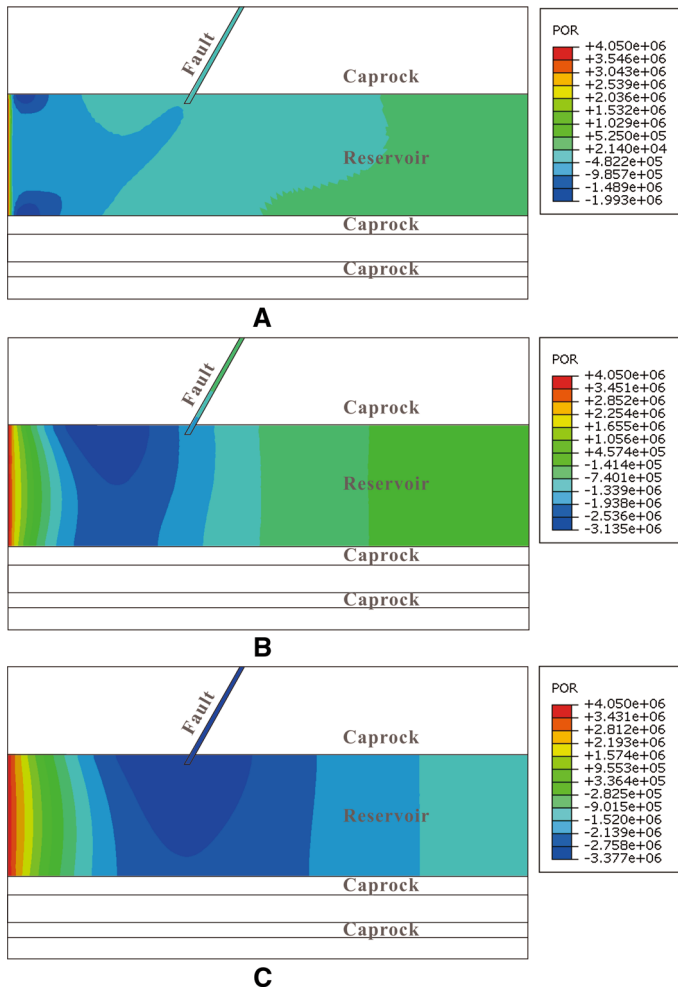
Fig. 2 A–C Pore pressure nephograms in the targeted reservoir and the fault at 1, 24, and 120 h, respectively

are useful for the modeling and analysis of engineering problems (Aslan and Cebeci 2007). RSM consists of a group of mathematical and statistical techniques based on the fit of empirical models to experimental data obtained in relation to the statistical experimental design. More specifically, RSM quantifies the relationship between the controllable input indicators, as well as their interactions, and the obtained response surfaces (Khuri and Mukhopadhyay 2010). In addition, the direct and interactive effects of the input indicators can be represented through two- and three-dimensional plots (Myers et al. 2009).

For this objective, linear or square polynomial functions were used to describe the studied system and consequently explore the experimental conditions until the system's optimization to achieve the minimalized Coulomb failure stress in the fault (Khuri and Mukhopadhyay 2010). Some of the stages in the application of RSM as an optimization technique are the following: (1) the selection of independent variables that exert major

effects on the system through screening studies and the delimitation of the statistical experimental region based on the experience of the researcher; (2) the choice of the experimental design and the performance of the experiments according to the selected experimental matrix; (3) the mathematic–statistical treatment of the obtained experimental data through fitting to a polynomial function; (4) the evaluation of model's fitness; (5) the verification of the necessity and possibility of performing a displacement in the direction toward the optimal region; and (6) the identification of the optimal values for each studied variable (Myers et al. 2009).

In most cases, tested parameters are not measurable. With the goal of optimizing the response variable, the independent variables were assumed to be controllable by experiments with negligible errors. Such a relationship between a response variable and the selection of independent tested parameters that exert major effects is unknown but can be approximated by a low-degree polynomial model of the form in which the response surface can be expressed as follows:

$$Y = K + \sum_{i=1}^{n} K_i x_i + \sum_{i=1}^{n} K_{ii} x_i^2 + \sum_{i=1}^{n-1} \sum_{j=1}^{n} K_{ij} x_i x_j + \varepsilon \tag{3}$$

where Y is the response variable; x_i and x_j are the tested parameters; $K, K_i, K_{ii},$ and K_{ij} are parameters that should be determined in a second-order model; and ε is a random error (Khuri and Mukhopadhyay 2010).

Optimizing refers to improving the performance of a system, a process, or a product in order to obtain the maximum benefit from it. The surfaces generated by linear models can be used to indicate the direction in which the original design must be displaced in order to attain the optimal conditions.

For quadratic models, the critical point can be characterized as maximum, minimum, or saddle. It is possible to calculate the coordinates of the critical point through the first derivate of the mathematical function, which describes the response surface and equates it to zero. The quadratic function obtained for two variables as described below (Eq. 4) is used to illustrate the example:

$$y = b_0 + b_1 x_1 + b_2 x_2 + b_{11} x_1^2 + b_{22} x_2^2 + b_{12} x_1 x_2 \tag{4}$$

$$\frac{\partial y}{\partial x_1} = b_1 + 2b_{11} x_1 + b_{12} x_2 = 0 \tag{5}$$

$$\frac{\partial y}{\partial x_2} = b_2 + 2b_{22} x_2 + b_{12} x_1 = 0 \tag{6}$$

Thus, to calculate the coordinate of the critical point, it is necessary to solve the first grade system formed by Eqs. (5) and (6) to find the x_1 and x_2 values. The visualization of the predicted model equation can be obtained by the surface response mapping. This graphical representation is an N-dimensional surface in the $(N + 1)$-dimensional space. Usually, a two-dimensional representation of a three-dimensional (3D) plot can be drawn. For the quadratic response surface plot in the optimization of two parameters, the location of the maximum point (inside the experimental region or outside the experimental region) determines the affection of parameter variation to the studied system. As a result, it is possible to find the optimum region through visual inspection of the surfaces.

3.2 Statistical experimental design for tests

The classical approach of changing one variable at a time and studying the effect of the variable on the response is a complicated technique, particularly in a multivariate system or in cases in which more than one response is important. Statistical experimental designs are statistical techniques that can be used to optimize such multivariable systems. Using a statistical experimental design based on response surface methodology, the aggregate mix proportions with the lowest void content can be determined with the minimum number of experiments without requiring the experimental study of all of the possible combinations. Furthermore, the input levels of the different variables for a particular response level can also be determined.

Response surface methodology can be applied when a response or a set of responses of interest is influenced by several variables. The objective is to simultaneously optimize the levels of these variables to attain the best system performance (Myers et al. 2009). However, before applying the RSM, it is first necessary to select a suitable statistical experimental design that will define which experiments should be performed in the experimental region being studied.

There are some experimental matrices for this purpose. In this study, based on the large number of 22-input input variables that exert major effects, we used a tornado analysis to determine which tested parameters have the greatest influence on the simulated results. A Box–Behnken experimental design for quadratic response surfaces can then be used to approximate a response function for the experimental data that cannot be described by linear functions.

3.2.1 Tornado analysis

A tornado analysis was used to determine which tested parameters have the greatest influence on the simulated resulting CFS generated with the fluid injection (O'Dell and Lindsey 2010). A tornado analysis was performed on the numerical model, which represented a column of five levels. Because only one simulated input indicator is changed at a time, 22-input tested parameters were varied to five levels, namely 60, 80, 100, 120, and 140 %, in the tornado analysis, as listed in Table 1. The ranges of the values for the subsurface uncertainties are based on observations and variations known for the caprock, fault, and reservoir properties observed in other CO_2 injection projects (Rohmer et al. 2014).

Based on the results listed in Appendix A in Supplementary Material, Fig. 3 shows the relative change in the CFS to the benchmark (100 % level) obtained in the tornado analysis. After eliminating the tested parameters that do not exert any significance (e.g., K_c and e_r) or do not show any observable sensitivity at a lower-value level (e.g., f and K_f), nine (P, φ_f, μ_c, φ_r, E_c, φ_c, K_r, μ_f, and E_f) out of the 22-input tested parameters were found to exert the greatest influence on the simulated CFS results. Moreover, it should be noted that the CFS value increases with increases in all of the nine tested parameters with the exception of the angle of friction in the reservoir (φ_r).

3.2.2 Box–Behnken experimental design

A statistical experimental design is widely used to control the effects of tested parameters in many processes. Its usage decreases the number of experiments and the use of time and

Table 1 Tested parameters and ranges in the tornado analysis

| Indicators		60 %	80 %	100 %	120 %	140 %
Injection pressure (MPa)	P	2.7	3.6	4.5	5.4	6.3
Coefficient of friction (1)	f	0.36	0.48	0.6	0.72	0.84
Stress field$^\$$ (1)	λ	0.3	0.4	0.5	0.6	0.7
Depth$^\#$ (m)	H	768	1020	1280	1540	1790
Caprock						
Young's modulus (GPa)	E_c	1.2	1.6	2	2.4	2.8
Poisson's ratio (1)	μ_c	0.18	0.24	0.3	0.36	0.42
Permeability (m^2)	K_c	6E−17	8E−17	1E−16	1.2E−16	1.4E−16
Void ratio (1)	e_c	0.06	0.08	0.1	0.12	0.14
Angle of friction (°)	φ_c	12	16	20	24	28
Dry density (kg/m^3)	ρ_c	960	1280	1600	1920	2690
Fault						
Young's modulus (GPa)	E_f	0.6	0.8	1	1.2	1.4
Poisson's ratio (1)	μ_f	0.18	0.24	0.3	0.36	0.42
Permeability (m^2)	K_f	6E−13	8E−13	1E−12	1.2E−12	1.4E−12
Void ratio (1)	e_f	0.06	0.08	0.1	0.12	0.14
Angle of friction (°)	φ_f	12	16	20	24	28
Dry density (kg/m^3)	ρ_f	960	1280	1600	1920	2690
Reservoir						
Young's modulus (GPa)	E_r	0.6	0.8	1	1.2	1.4
Poisson's ratio (1)	μ_r	0.18	0.24	0.3	0.36	0.42
Permeability (m^2)	K_r	6E−11	8E−11	1E−10	1.2E−10	1.4E−10
Void ratio (1)	e_r	0.06	0.08	0.1	0.12	0.14
Angle of friction (°)	φ_r	12	16	20	24	28
Dry density (kg/m^3)	ρ_r	960	1280	1600	1920	2690

$^\$$ Lateral stress coefficient

$^\#$ Depth of top surface of the reservoir

material resources (Ferreira et al. 2007). A Box–Behnken statistical screening design was used to statistically optimize the formulation tested parameters and evaluate their main effects K_i, interaction effects K_{ij}, and quadratic effects K_{ii} in Eq. (3) to the Coulomb failure stress and moment magnitude of the induced seismicity (Rohmer 2014). This cubic design is characterized by a set of points lying at the midpoint of each edge of a multidimensional cube and center point replicates, and the 'missing corners' help the experimenter avoid the combined factor extremes. This property prevents a potential loss of data in these cases (Box and Behnken 1960).

In this study, based on statistical diversity, the full factorial statistical experimental design of the nine tested parameters, which were varied at the three levels listed in Table 2, would result in a detailed response surface after considerable computational work. With the expectation of a detailed response, note that a full factorial design requires the evaluation of all of the possible combinations of the nine tested parameters at the high, middle, and low levels and requires $3^9 = 19,683$ simulation runs to implement. Thus, a huge workload and long working hours would be required to complete these simulation runs before the application of an efficient statistical experimental design.

Fig. 3 Relative change in the CFS obtained in the tornado analysis
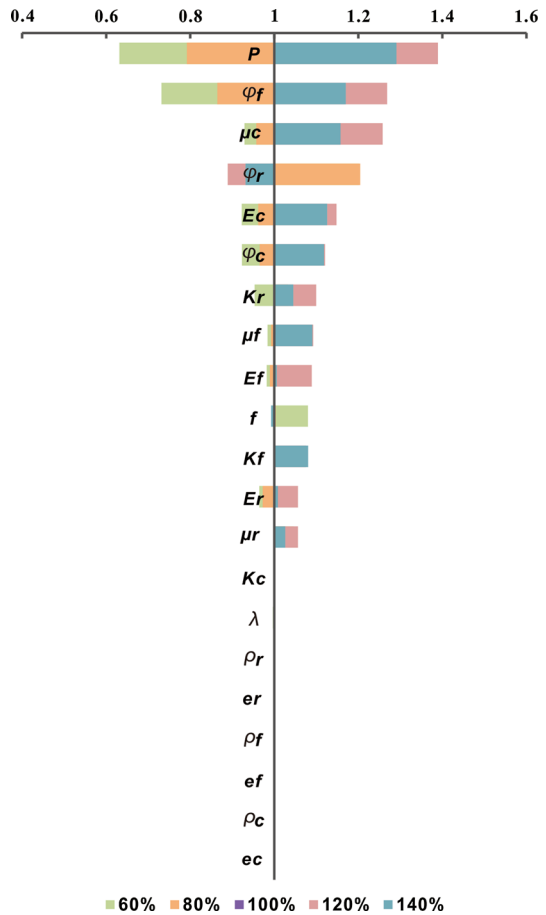
Table 2 Nine impact indicators varied in three levels

Impact indicators		90 %	100 %	110 %
Injection pressure (MPa)	P	4.05	4.5	4.95
Angle of friction in the fault (°)	φ_f	18	20	22
Poisson's ratio in the caprock (1)	μ_c	0.27	0.3	0.33
Angle of friction in the reservoir (°)	φ_r	18	20	22
Young's modulus in the caprock (GPa)	E_c	1.8	2	2.2
Angle of friction in the caprock (°)	φ_c	18	20	22
Permeability in reservoir (E−10 m²)	K_r	0.9	1	1.1
Poisson's ratio in the fault (1)	μ_f	0.27	0.3	0.33
Young's modulus in the fault (GPa)	E_f	0.9	1	1.1

The Box–Behnken experimental design (BBD) is a class of rotatable or nearly rotatable second-order designs based on three-level incomplete factorial designs. For three factors, its graphical representation can be seen in two forms: a cube that consists of the

central point and the middle points of the edges and a figure of three interlocking 22 factorial designs and a central point (Zhou and Burbey 2014). The number of experiments (N) required for the development of BBD is defined as $N = 2\,k(k - 1) + C_0$, (where k is number of factors and C_0 is the number of central points). For comparison, the number of experiments for a central composite design is $N = 2k + 2k + C_0$. BBD is slightly more efficient than the central composite design but much more efficient than the three-level full factorial designs where the efficiency of one experimental design is defined as the number of coefficients in the estimated model divided by the number of experiments. The Box–Behnken is a good design for response surface methodology because it permits the following: (1) estimation of the tested parameters of the quadratic model; (2) building of sequential designs; (3) detection of a lack of fit of the model; and (4) the use of blocks (Ferreira et al. 2007). Another advantage of the BBD is that it does not contain combinations for which all factors are simultaneously at their highest or lowest levels. So these designs are useful in avoiding experiments performed under extreme conditions, for which unsatisfactory results might occur (Coussy 2004).

To decrease the number of simulation runs, a spreadsheet implementation of the Box–Behnken design, which creates an evenly spaced lattice of the input variable combinations, is available (Ferreira et al. 2007). Therefore, the Box–Behnken experimental design was chosen to determine the relationship between the response functions and the variables. For a three-level nine-factorial Box–Behnken experimental design, a total of 130 experimental runs are needed. The runs were generated using simulation software (Shen 2010). The response functions can be directly calculated with a user-defined subroutine, and selected simulation results were gathered from each of the runs and used for the statistical analysis process (Appendix B in Supplementary Material).

4 Results and discussion

4.1 Uncertainty analysis of the Coulomb failure stress

4.1.1 Statistical significance of the indicators of Coulomb failure stress

In geosequestration, the injection pressure in conjunction with the upward pressure exerted by the injected CO_2 (due to buoyant forces) leads to perturbation of the stress field in the reservoir. The change in Coulomb failure stress of the reservoir formation rock and caprock caused by the perturbation can lead to strength reduction and failure of the caprock. For this reason, the level of Coulomb failure stress was raised as a predicted response of variables to evaluate the caprock integrity, and the present investigation was carried out to minimize the Coulomb failure stress to a practical lower level and to optimize the mix proportion of the individual variables (Shukla et al. 2010).

The present investigation was conducted to minimize the Coulomb failure stress to a practical lower level and to optimize the mix proportion of the individual variables. As shown in Appendix B in Supplementary Material, the Coulomb failure stress (response) of the 130 statistically designed combinations (inputs) suggested by the Box–Behnken design of experiments for the nine variables was experimentally determined, and the minimum and maximum CFS values obtained were 3.412 MPa and 5.404 MPa, respectively. The application of the response surface methodology yielded a regression equation from an analysis of the variance that gave the level of Coulomb failure stress as a predicted

response of the variables and fits the experimental data with a correlation coefficient (R^2) of 0.9757, indicating that the fitness of the selected model is good and that the model could be used for further investigation.

$$
\begin{aligned}
CFS \; = \; & -4316260 - 531465 * P + 202750 * \varphi_r - 317650 * \varphi_f \\
& - 337475 * \mu_c - 176610 * \varphi_c - 185765 * \mu_f - 458450 * P * \varphi_c \\
& + 425950 * P * \mu_f - 586999 * \mu_c * E_c + 457499 * \mu_c * \varphi_c \\
& - 480999 * E_c * \varphi_c - 529950 * \varphi_c * \mu_f
\end{aligned}
\tag{7}
$$

The main effects (K_i) and reciprocal actions (K_{ii} and K_{ij}) in Eq. (7) were estimated from the experimental results. All of the terms, in consideration of their significance, were included in the equation above. The practical application of this statistical model is to link the results obtained from Box–Behnken experimental design to response surface methodology. It concluded the relation between the 130 combinations of the 3 leveled 9 parameters and their corresponding Coulomb failure stress in the first place, and the statistical significance of indicators on Coulomb failure stress as well as optimum design for minimum Coulomb failure stress are all based on this model.

An analysis of variance (ANOVA) of the response surface quadratic model gives the squares and degrees of freedom for the regression Eq. (4). In statistics, the P value (not variable P in Eq. (7)) is a function of the observed sample results and is used to test a statistical hypothesis. Before performing the test, a threshold value is chosen, called the significance level of the test, which was 5 % in this study and denoted as α (Nuzzo 2014). A P value equal to or smaller than the significance level (α) suggests that the observed data are inconsistent with the assumption that the null hypothesis is true and thus that the hypothesis must be rejected, resulting in the alternative hypothesis being accepted as true (Iversen and Norpoth 1987). When the P value is calculated correctly, such a test is guaranteed to maintain the error rate at a value no greater than α. Therefore, the P value level indicates the significant model terms, and a model P value less than 0.0001 indicates that the tested parameters are significant. In contrast, a model P value greater than 0.05 indicates that the tested parameters are not significant. Moreover, the F test is used to compare the components of the total deviation because statistical significance is tested by comparing the F test statistic, the F value of the quadratic model, and individual model terms. An ANOVA of the response surface quadratic model gives the squares and degrees of freedom for the 130 combinations and the corresponding Coulomb failure stress, as listed in Appendix C in Supplementary Material. Moreover, the F test is used to compare the components of the total deviation because statistical significance is tested by comparing the F test statistic, the F value of the quadratic model, and individual model terms. Based on the ANOVA results, the sensitivity and reciprocal action of the impact indicators are shown in Fig. 4.

As shown in Fig. 4, the injection pressure, Poisson's ratio in the caprock, and angle of friction in the fault are highly significant to the level of Coulomb failure stress with a P value at the 0.001 level; Poisson's ratio in the caprock * Young's modulus in the caprock, angle of friction in the caprock * Poisson's ratio in the fault, Young's modulus in the caprock * angle of friction in the caprock, and injection pressure * angle of friction present significance at the 0.01 level; angle of friction in the reservoir, Poisson's ratio in the fault and angle of friction in the caprock exhibit significance at the 0.05 level; and none of the other tested parameters are significant ($P > 0.05$) to the predicted response. Additional tested parameters with P value greater than 1 are not listed in the histogram.
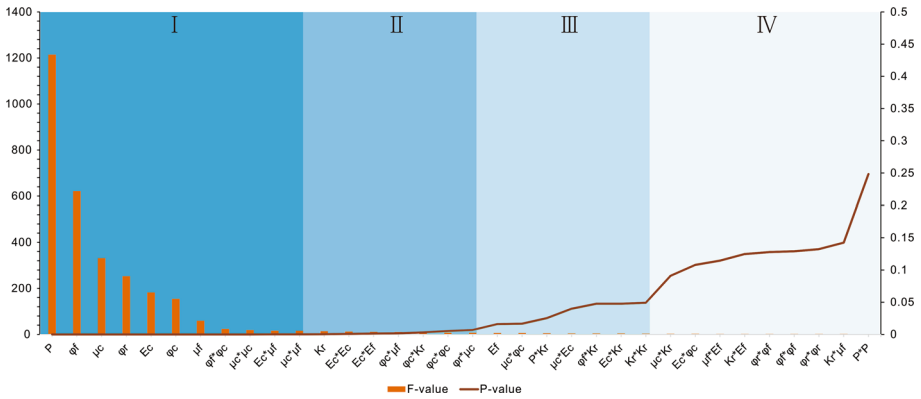
Fig. 4 Sensitivity and reciprocal action of the tested parameters. The color depth of the four partitions (*I*, *II*, *III* and *IV*) in the *histogram* indicates their significance level from high to low. In each partition, the sensitivity and reciprocal action of the tested parameters are listed by their *F* value as follows: tested parameters in (*I*) are highly significant to the level of Coulomb failure stress with a *P* value at the 0.001 level; the *P* values in (*II*) and (*III*) are at the 0.01 and 0.05 levels, respectively; and *P* values greater than 0.05 in (*IV*) indicate no significance

4.1.2 Optimal design of indicators of Coulomb failure stress

To better understand the results, the predicted models are presented in Fig. 5 as 3D response surface plots. Figure 5 shows the reciprocal action of the highly significant indicators injection pressure (*P*), Poisson's ratio in the caprock (μ_c), and angle of friction in the fault (φ_f) to the Coulomb failure stress.

As shown in Fig. 5A, B, C, as the coded values of the proportion of injection pressure, Poisson's ratio in the caprock, and the angle of friction in the fault increase from −1 to 1, the Coulomb failure stress increases. This result indicates that the injection pressure, Poisson's ratio in the caprock, and angle of friction in the fault significantly increase the Coulomb failure stress. In particular, as the most sensitive indicator, an increase in the injection pressure within the range results in a greater increase in Coulomb failure stress.

To minimize the Coulomb failure stress to a practical lower level and to optimize the mix proportion of the individual variables, optimization was accomplished by obtaining the individual optimal values for each response and by combining the individual optima to obtain a combined or composite optimum and later maximizing the composite optimum and identifying the optimal tested parameters settings. The predicted Coulomb failure stress was obtained from the regression equation using the experimentally determined values for the 130 combinations. Upon optimization, a minimization target was assigned to the resolution factor response CFS value in numerical optimization. Accordingly, the minimum Coulomb failure stress given by the computation software was −3.39331 MPa. The optimal levels of the coded individual variables to minimize the CFS are shown in Fig. 6.

As the proportion of the tested parameters reached their individual optimal coded values, the CFS decreased to −3.39331 MPa, corresponding to the optimal value. In particular, a desirability value of 1.000 indicates a good fit of the predictive model. Furthermore, the optimized combination was significantly different from the experimentally studied combinations and showed less CFS. This result demonstrates the usefulness of
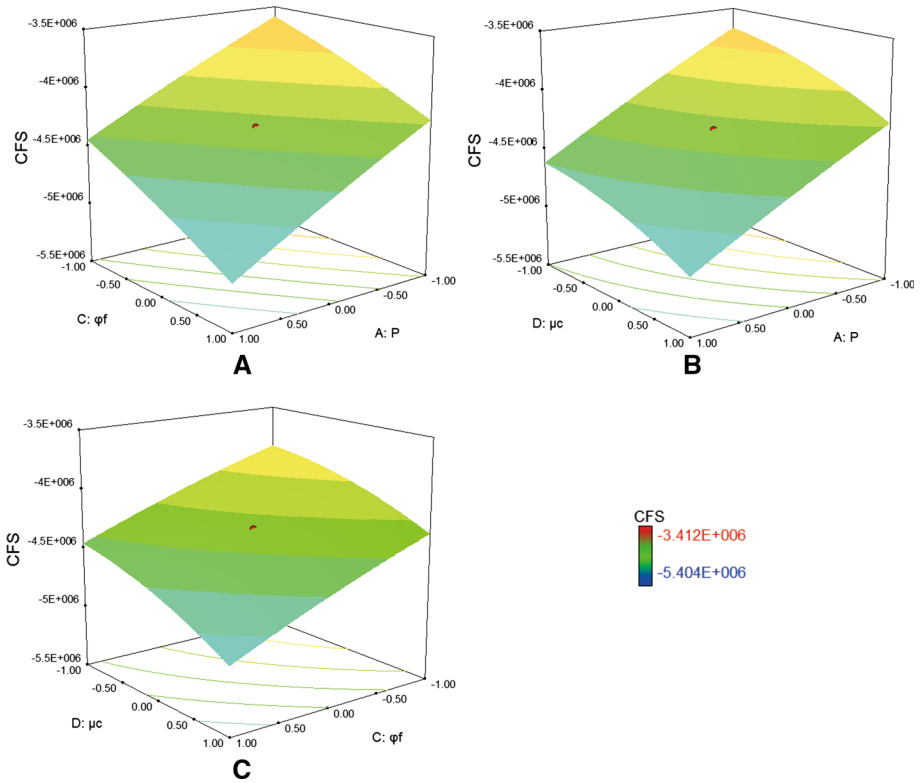
Fig. 5 Predicted models of highly significant indicators of CFS. The 3D response surface plot showing the effect of injection pressure and Poisson's ratio in the caprock in **A** indicates that increases in the coded values of the proportion of injection pressure and Poisson's ratio in the caprock from −1 to 1 increase the Coulomb failure stress. The effect of injection pressure and angle of friction in the fault is shown in **B**, and the effect of Poisson's ratio in the caprock and angle of friction in the fault is shown in **C**. Increases in the values of the proportion of injection pressure, Poisson's ratio in the caprock, and angle of friction in the fault from −1 to 1 in Fig. 5A, B, C increase the Coulomb failure stress to −5.404 MPa and thereafter continues to increase. This result indicates that the injection pressure, Poisson's ratio in the caprock, and angle of friction in the fault maximize the Coulomb failure stress

Fig. 6 Optimal levels of the coded individual variables to minimize the CFS
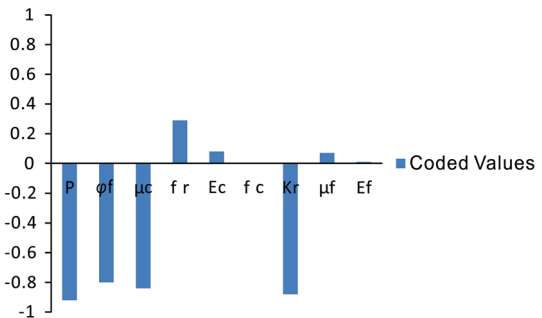
statistical techniques in model exploitation and empirical model building. The final optimal design for the subsurface uncertainties in terms of actual indicator values is shown in Table 3.

Table 3 Actual tested parameters' values in the optimal design for the subsurface uncertainties

Impact indicators		Coded values	Range	Actual values
Injection pressure (MPa)	P	−0.92	4.05–4.95	4.086
Angle of friction in the fault (°)	φ_f	−0.8	18–22	18.4
Poisson's ratio in the caprock (1)	μ_c	−0.84	0.27–0.33	0.2748
Angle of friction in the reservoir (°)	φ_r	0.29	18–22	20.58
Young's modulus in the caprock (GPa)	E_c	0.08	1.8–2.2	2
Angle of friction in the caprock (°)	φ_c	0	18–22	20
Permeability in reservoir (E−10 m^2)	K_r	−0.88	0.9–1.1	0.912
Poisson's ratio in the fault (1)	μ_f	0.07	0.27–0.33	0.3021
Young's modulus in the fault (GPa)	E_f	0.01	0.9–1.1	1.001

4.2 Uncertainty analysis of moment magnitude

4.2.1 Seismic moment and moment magnitude

The scalar seismic moment M_0, as defined for a ruptured patch on a fault by Hanks and Kanamori (1979), is as follows:

$$M_0 = GAd \tag{8}$$

where G is the shear modulus, A is the rupture area, and d is the average slip in the rupture area. Second, the moment magnitude M_w of an earthquake is given by Kanamori and Anderson (1975) as follows:

$$M_w = \frac{2}{3}(\log_{10}(M_0) - 9.1) \tag{9}$$

Note that our simulation results were achieved with a 2D plane-strain model, and to calculate the seismic moment and magnitude, the length of the rupture area A was 200 m, but the depth of the rupture area A was assumed. In this model, the shear modulus G can be easily calculated with the Young's modulus and Poisson's ratio provided above by the equation $G = E/2(1 + \mu) = 7.69E + 09$.

### 4.2.2 Statistical significance of the indicators of moment magnitude

From the application of the Box–Behnken experimental design and response surface methodology, the minimum and maximum moment magnitude (M_w) values obtained were 4.17986 and 4.36532. The regression equation obtained after the analysis of variance gave the level of M_w as a predicted response of the variables. This equation fitted the experimental data best with a correlation coefficient (the value of R^2) of 0.9946. The main effects (K_i) and reciprocal actions (K_{ii}, K_{ij}) in Eq. (3) were estimated from the experimental results. All of the terms, regardless of their significance, were included in the following equation:

$$
\begin{aligned}
M_w = {} & 4.270933965 + 0.007172216 * P + 0.043785571 * \varphi_r + 0.00986756 * \varphi_f \\
& + 0.028086374 * \mu_c + 0.021237674 * E_c + 0.017992779 * \varphi_c + 0.032056121 * K_r \\
& + 0.00095415 * \mu_f + 0.00291713 * P * \varphi_r + 0.00166024 * P * K_r \\
& + 0.00409613 * \varphi_r * K_r - 0.001646151 * \varphi_r^2 - 0.002296648 * \varphi_f^2 \\
& + 0.001731633 * \mu_c^2 - 0.001241751 * E_c^2 - 0.001714995 * K_r^2
\end{aligned}
\tag{10}
$$

An analysis of variance (ANOVA) for the response surface quadratic model gives the squares and degrees of freedom for the 130 combinations and corresponding M_w values listed in Appendix B in Supplementary Material. Based on the ANOVA results, the sensitivity and reciprocal action of the tested parameters are shown in Fig. 7. The injection pressure, Poisson's ratio in the caprock, and angle of friction in the fault are highly significant to the M_w level with a P value at the 0.001 level; Poisson's ratio in the caprock * Young's modulus in the caprock, angle of friction in the caprock * Poisson's ratio in the fault, Young's modulus in the caprock * angle of friction in the caprock, and injection pressure * angle of friction present significance at the 0.01 level; the angle of friction in the reservoir, Poisson's ratio in the fault, and angle of friction in the caprock are significant tested parameters at the 0.05 level; and none of the other indicators are significant ($P > 0.05$) for the predicted response. Additional tested parameters with a P value greater than 1 are not listed in the histogram. The detailed ANOVA results are listed in Appendix D in Supplementary Material.

4.2.3 Optimal design of indicators of the moment magnitude

The effect of the three highly significant tested parameters, namely angle of friction in the reservoir (φ_r), permeability in the reservoir (K_r) and Poisson's ratio in the caprock (μ_c), on the M_w is shown in Fig. 8A–C. Increases in the coded values of the proportion of the angle of friction in the reservoir, the permeability in the reservoir, and Poisson's ratio in the
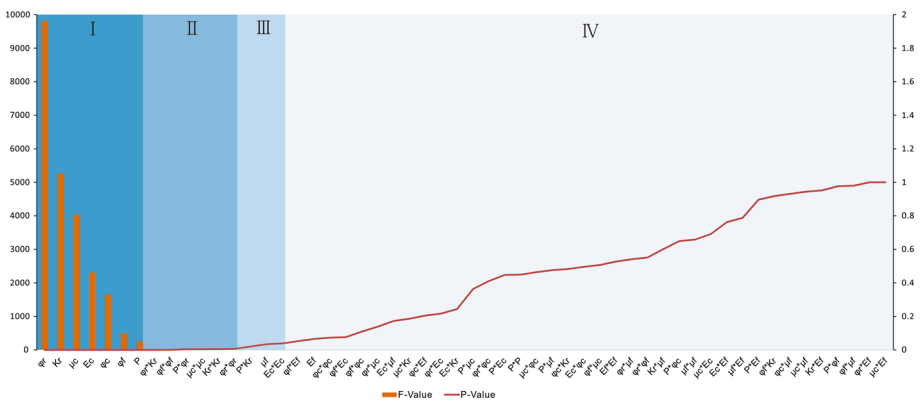
Fig. 7 Sensitivity and reciprocal action of the impact indicators. The color depth of the four partitions *I, II, III* and *IV* in the *histogram* indicates their significance level from high to low. In each partition, the sensitivity and reciprocal action of the tested parameters are listed by their *F* value as follows: the tested parameters in (*I*) are highly significant to the M_w level with a *P* value at the 0.001 level; the *P* values in (*II*) and (*III*) are at the 0.01 and 0.05 levels, respectively; and the *P* values greater than 0.05 in (*IV*) indicate no significance
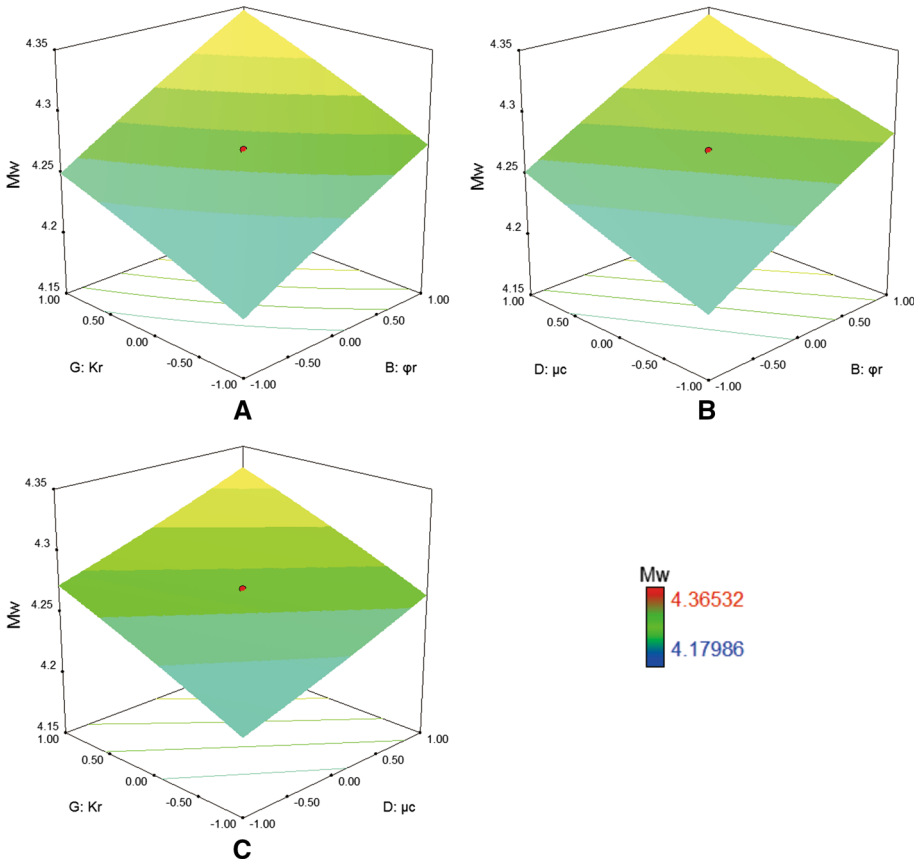
Fig. 8 Predicted models of highly significant indicators of M_w. The 3D response surface plot showing the effect of injection pressure and Poisson's ratio in the caprock in **A** indicates that increases in the coded values of the proportion of the angle of friction in the reservoir (φ_r) and the permeability in the reservoir (K_r) from −1 to 1 increase the M_w. The effect of the permeability in the reservoir (K_r) and Poisson's ratio in the caprock (μ_c) is shown in **B**, and the effect of the angle of friction in the reservoir (φ_r) and Poisson's ratio in the caprock (μ_c) is shown in **C** Increases in the proportion of the injection pressure, Poisson's ratio in the caprock, and the angle of friction in the fault from −1 to 1 in **A–C** increase the M_w, which continues to increase thereafter. This result indicates that the angle of friction in the reservoir, permeability in the reservoir, and Poisson's ratio in the caprock maximize the M_w

caprock from −1 to 1 increase the M_w. This result indicates that the friction in the reservoir, the permeability in the reservoir, and Poisson's ratio in the caprock significantly increase the M_w. In particular, as the most sensitive indicator, the angle of friction in the reservoir has the largest of the chosen sizes, and higher input values will lessen the values required for other grades to fill the high M_w level.

The present investigation was conducted to minimize the M_w to a practical lower level and to optimize the mix proportion of the individual variables. The predicted M_w was obtained from the regression equation using the experimentally determined values for the 130 combinations. A minimization target was assigned to the resolution factor response M_w in the numerical optimization. Accordingly, the minimum M_w given by the software was 4.17339. The optimal levels of the coded individual variables for minimizing the M_w are shown in Fig. 9.

The M_w decreased to 4.17339 when the proportion of tested parameters reached their individual optimal coded values, and the desirability value of 1.000 shows a good fit of the predictive model. Furthermore, the difference between the optimized combination and the studied combinations showed a lower M_w, demonstrating the usefulness of statistical techniques in model exploitation and empirical model building. The final optimal design for the subsurface uncertainties in terms of the actual tested parameters values is shown in Table 4.

5 Conclusions

The optimization of tested impact parameters is a complex process that requires one to consider a large number of variables and their interactions. The present study conclusively demonstrates the application of response surface methodology, and the use of the Box–Behnken design from the point of tested impact parameters for caprock integrity during CO_2 injection was discussed.

A suitable approximation for the true functional relationships between independent tested parameters and the response surfaces was obtained from a limited number of experimental runs and was in good agreement with the experimental values of both Coulomb failure stress and moment magnitude of the induced seismicity. An analysis of variance of this response surface quadratic model gives the sum of squares and degrees of freedom for the model for estimating the statistical significance of tested parameters of the Coulomb failure stress and moment magnitude of the corresponding seismicity. In addition, response surface mapping aids the prediction of the values of selected independent variables for the preparation of optimal formulations with desired properties. We therefore reached the following conclusions:

1. The results of an analysis of variance of the response surface quadratic model demonstrated that the injection pressure, angle of friction in the fault, Poisson's ratio in the caprock, angle of friction in the reservoir, Young's modulus in the caprock, angle of friction in the caprock, Poisson's ratio in the fault, and the quadratic term angle of friction in the fault * angle of friction in the caprock are highly significant to the level of Coulomb failure stress with a P value at the 0.001 level. In addition, the angle of friction in the reservoir, permeability in the reservoir, Poisson's ratio in the caprock, Young's modulus in the caprock, angle of friction in the caprock, angle of friction in the fault, injection pressure, and the quadratic terms angle of friction in the reservoir * permeability in the reservoir, Poisson's ratio in the caprock * Poisson's ratio in the

Fig. 9 Optimal levels of the coded tested parameters for minimizing the M_w
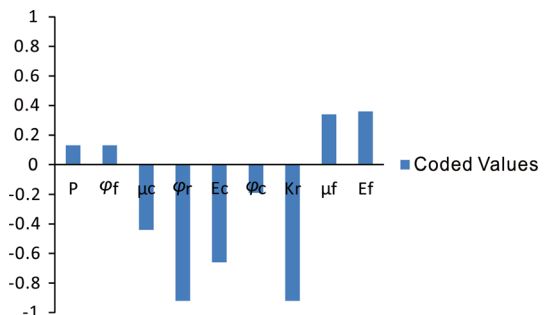
Table 4 Actual tested parameters' values in the optimal design for the subsurface uncertainties

Impact indicators		Coded values	Range	Actual values
Injection pressure (MPa)	P	0.13	4.05–4.95	4.5585
Angle of friction in the fault (°)	φ_f	0.13	18–22	20.26
Poisson's ratio in the caprock (1)	μ_c	−0.44	0.27–0.33	0.2868
Angle of friction in the reservoir (°)	φ_r	−0.92	18–22	18.16
Young's modulus in the caprock (GPa)	E_c	−0.66	1.8–2.2	1.6812
Angle of friction in the caprock (°)	φ_c	−0.19	18–22	19.62
Permeability in reservoir (E−10 m^2)	K_r	−0.92	0.9–1.1	0.908
Poisson's ratio in the fault (1)	μ_f	0.34	0.27–0.33	0.3102
Young's modulus in the fault (GPa)	E_f	0.36	0.9–1.1	1.036

caprock, Young's modulus in the caprock * Poisson's ratio in the fault, and Poisson's ratio in the caprock * Poisson's ratio in the fault are highly significant to the M_w level of the induced seismicity with a P value at the 0.001 level.

2. The highly significant tested parameters of the Coulomb failure stress and moment magnitude of the induced seismicity are listed in an inconsistent sequence. For Coulomb failure stress, injection pressure is the most sensitive indicator, and variations in the value of the injection pressure lead to significant changes in the Coulomb failure stress. However, for the M_w of the induced seismicity, the tested parameters in the reservoir and the caprock play a key role. Due to the above conclusions, we should focus on controlling the magnitude of the injection pressure to avoid caprock failure in most CCS projects, but for the projects that have demonstrated that induced seismicity may indeed occur, such as Weyburn in Saskatchewan, Canada, In Salah in Algeria, and Sleipner in the Norwegian sector of the North Sea, we should not only evaluate the injection pressure but also choose the optimal geomechanical conditions. In addition to both Coulomb failure stress and the moment magnitude of the induced seismicity, the tested parameters in the fault are not as significant as those in the reservoir and the caprock due to the relatively small volume of the fault in the whole model.

3. Both the Coulomb failure stress and the moment magnitude of the induced seismicity for different combinations of subsurface uncertainties were optimized based on the experimental data. The optimal combinations had a predicated value of less than the experimentally determined model with a desirability value of 1.000, which demonstrated the fitness of the statistical model for analyzing the experimental data. Furthermore, this study demonstrated that the Box–Behnken design and response surface methodology can efficiently be applied for the modeling of caprock integrity during CO_2 injection and that this approach is an economical method for obtaining the maximal amount of information in a short period of time and with the fewest number of experimental runs. However, due to the problem of convergence, we have to compromise the uncertainty range (90–110 %) to ensure our results are usable and accurate in this study. We can account for larger levels of uncertainty for future lines of research and application.

References

Aruffo C, Rodriguez-Herrera A, Tenthorey E, Krzikalla F, Minton J, Henk A (2014) Geomechanical modelling to assess fault integrity at the CO2CRC Otway project, Australia. Aust J Earth Sci 61:987–1001

Aslan N, Cebeci Y (2007) Application of Box–Behnken design and response surface methodology for modeling of some Turkish coals. Fuel 86:90–97. doi:10.1016/j.fuel.2006.06.010

Bachu S (2000) Sequestration of CO_2 in geological media: criteria and approach for site selection in response to climate change. Energy Convers Mgmt 41:953–970

Biot MA (1956) Theory of propagation of elastic waves in a fluid-saturated porous solid. I. Low-frequency range. J Acoust Soc Am 28:168–178

Box GEP, Behnken DW (1960) Some new three level designs for the study of quantitative variables. Technometrics 2:455–475. doi:10.1080/00401706.1960.10489912

Box GE, Hunter JS (1957) Multi-factor experimental designs for exploring response surfaces. Ann Math Stat 195–241

Cappa F, Rutqvist J (2011) Modeling of coupled deformation and permeability evolution during fault reactivation induced by deep underground injection of CO_2. Int J Greenh Gas Control 5:336–346

Coussy O (2004) Poromechanics. Wiley, New York

Dempsey D, Kelkar S, Pawar R, Keating E, Coblentz D (2014) Modeling caprock bending stresses and their potential for induced seismicity during CO_2 injection. Int J Greenh Gas Control 22:223–236. doi:10.1016/j.ijggc.2014.01.005

Deng H, Stauffer PH, Dai Z, Jiao Z, Surdam RC (2012) Simulation of industrial-scale CO_2 storage: multi-scale heterogeneity and its impacts on storage capacity, injectivity and leakage. Int J Greenh Gas Control 10:397–418. doi:10.1016/j.ijggc.2012.07.003

Dethlefsen F, Haase C, Ebert M, Dahmke A (2011) Uncertainties of geochemical modeling during CO_2 sequestration applying batch equilibrium calculations. Environ Earth Sci 65:1105–1117. doi:10.1007/s12665-011-1360-x

Fei W, Li Q, Wei X, Song R, Jing M, Li X (2015) Interaction analysis for CO_2 geological storage and underground coal mining in Ordos Basin, China. Eng Geo 196:194–209. doi:10.1016/j.enggeo.2015.07.017

Ferreira SL et al (2007) Box–Behnken design: an alternative for the optimization of analytical methods. Anal Chim Acta 597:179–186. doi:10.1016/j.aca.2007.07.011

Gysi AP, Stefánsson A (2012) Experiments and geochemical modeling of CO_2 sequestration during hydrothermal basalt alteration. Chem Geol 306–307:10–28. doi:10.1016/j.chemgeo.2012.02.016

Hosein R, Alshakh S (2013) CO_2 sequestration in saline water: an integral part of CO_2 sequestration in a geologic formation. Pet Sci Technol 31:2534–2540. doi:10.1080/10916466.2011.574181

IPCC (2005) IPCC special report on carbon dioxide capture and storage. Cambridge University Press, Cambridge

Iversen GR, Norpoth H (1987) Analysis of variance, vol 1. Sage, London

Jaeger JC, Cook NG, Zimmerman R (2009) Fundamentals of rock mechanics. Wiley, New York

Jeannin L, Mainguy M, Masson R, Vidal-Gilbert S (2007) Accelerating the convergence of coupled geomechanical-reservoir simulations. Int J Numer Anal Meth Geomech 31:1163–1181. doi:10.1002/nag.576

Karimnezhad M, Jalalifar H, Kamari M (2014) Investigation of caprock integrity for CO_2 sequestration in an oil reservoir using a numerical method. J Nat Gas Sci Eng 21:1127–1137. doi:10.1016/j.jngse.2014.10.031

Khuri AI, Mukhopadhyay S (2010) Response surface methodology. Wiley Interdiscip Rev Comput Stat 2:128–149. doi:10.1002/wics.73

Lary LD et al. (2015) Quantitative risk assessment in the early stages of a CO_2 geological storage project: implementation of a practical approach in an uncertain context. Greenh Gases Sci Technol 5:50–63. doi:10.1002/ghg.1447

Lei X, Ma S (2013) A detailed view of the injection-induced seismicity in a natural gas reservoir in Zigong, southwestern Sichuan Basin, China. J Geophys Res Solid Earth 118:4296–4311

Li Q, Liu G, Liu X, Li X (2013) Application of a health, safety, and environmental screening and ranking framework to the Shenhua CCS project. Int J Greenh Gas Control 17:504–514. doi:10.1016/j.ijggc.2013.06.005

Li Q, Fei W, Liu X, Wei X, Jing M, Li X (2014a) Challenging combination of CO_2 geological storage and coal mining in the Ordos Basin, China. Greenh Gases Sci Technol 4:452–467. doi:10.1002/ghg.1408

Li Q, Liu G, Liu X (2014b) Development of management information system of global acid gas injection projects. In: Wu Y, Carroll JC, Li Q (eds) Gas injection for disposal and enhanced recovery. Advances in natural gas engineering. Wiley, New York, pp 243–254. doi:10.1002/9781118938607.ch13

Li Q, Wei Y-N, Liu G, Lin Q (2014c) Combination of CO_2 geological storage with deep saline water recovery in western China: insights from numerical analyses. Appl Energy 116:101–110. doi:10.1016/j.apenergy.2013.11.050

Liu L-C, Wu G (2015) Assessment of energy supply vulnerability between China and USA. Nat Hazards 75:127–138. doi:10.1007/s11069-014-1071-1

Liu C, Zhao H, Sun Y (2009) Tectonic background of Ordos Basin and its controlling role for basin evolution and energy mineral deposits. Energy Explor Exploit 27:15–27

Mathias SA, Hardisty PE, Trudell MR, Zimmerman RW (2009) Screening and selection of sites for CO_2 sequestration based on pressure buildup. Int J Greenh Gas Control 3:577–585

Myers RH, Montgomery DC, Anderson-Cook CM (2009) Response surface methodology: process and product optimization using designed experiments, vol 705. Wiley, New York

Nuzzo RG (2014) Scientific method: statistical errors. Nature 506:150–152

O'Dell PM, Lindsey KC (2010) Uncertainty management in a major CO_2 EOR project. Abu Dhabi International Petroleum Exhibition and Conference. Society of Petroleum Engineers, Abu Dhabi, UAE. doi:10.2118/137998-MS

Rohmer J (2014) Induced seismicity of a normal blind undetected reservoir-bounding fault influenced by dissymmetric fractured damage zones. Geophys J Int 197:636–641. doi:10.1093/gji/ggu018

Rohmer J et al (2014) Improving our knowledge on the hydro-chemo-mechanical behaviour of fault zones in the context of CO_2 geological storage. Energy Procedia 63:3371–3378. doi:10.1016/j.egypro.2014.11.366

Rutqvist J (2012) The geomechanics of CO_2 storage in deep sedimentary formations. Geotech Geol Eng 30:525–551. doi:10.1007/s10706-011-9491-0

Rutqvist J, Wu YS, Tsang CF, Bodvarsson G (2002) A modeling approach for analysis of coupled multiphase fluid flow, heat transfer, and deformation in fractured porous rock. Int J Rock Mech Min Sci 39:429–442

Seebeck H, Tenthorey E, Consoli C, Nicol A (2015) Polygonal faulting and seal integrity in the Bonaparte Basin, Australia. Mar Pet Geol 60:120–135. doi:10.1016/j.marpetgeo.2014.10.012

Shen X (2010) Examples and applications of ABAQUS in energy engineering. China Machine Press, Beijing

Shukla R, Ranjith P, Haque A, Choi X (2010) A review of studies on CO_2 sequestration and caprock integrity. Fuel 89:2651–2664. doi:10.1016/j.fuel.2010.05.012

Song J, Zhang D (2013) Comprehensive review of caprock-sealing mechanisms for geologic carbon sequestration. Environ Sci Technol 47:9–22. doi:10.1021/es301610p

Tenthorey E, Dance T, Cinar Y, Ennis-King J, Strand J (2014) Fault modelling and geomechanical integrity associated with the CO2CRC Otway 2C injection experiment. Int J Greenh Gas Control 30:72–85. doi:10.1016/j.ijggc.2014.08.021

Vidal-Gilbert S, Nauroy J-F, Brosse E (2009) 3d geomechanical modelling for CO_2 geologic storage in the Dogger carbonates of the Paris Basin. Int J Greenh Gas Control 3:288–299. doi:10.1016/j.ijggc.2008.10.004

Vilarrasa V (2014) Impact of CO_2 injection through horizontal and vertical wells on the caprock mechanical stability. Int J Rock Mech Min Sci 66:151–159. doi:10.1016/j.ijrmms.2014.01.001

Wei XC, Li Q, Li X-Y, Sun Y-K, Liu XH (2015) Uncertainty analysis of impact indicators for the integrity of combined caprock during CO_2 geosequestration. Eng Geol 196:37–46. doi:10.1016/j.enggeo.2015.06.023

Xing H, Liu Y, Gao J, Chen S (2015) Recent development in numerical simulation of enhanced geothermal reservoirs. J Earth Sci 26:28–36

Yang D, Zeng R, Zhang Y, Wang Z, Wang S, Jin C (2012) Numerical simulation of multiphase flows of CO_2 storage in saline aquifers in Daqingzijing oilfield, China. Clean Technol Environ Policy 14:609–618. doi:10.1007/s10098-011-0420-y

Zhou X, Burbey TJ (2014) Pore-pressure response to sudden fault slip for three typical faulting regimes. Bull Seismol Soc Am 104:793–808

Zhou R, Huang L, Rutledge J (2010) Microseismic event location for monitoring CO_2 injection using double-difference tomography. Lead Edge 29:208–214. doi:10.1190/1.3304826

Zoback MD, Gorelick SM (2012) Earthquake triggering and large-scale geologic storage of carbon dioxide. Proc Natl Acad Sci USA 109:10164–10168. doi:10.1073/pnas.1202473109